S···S and S···P chalcogen bonding in solution : a cryospectroscopic study of the complexes of 2,2,4,4-tetrafluoro-1,3-dithietane with dimethyl sulfide and trimethylphosphine

Reference:

Geboes Yannick, De Vos Elias, Herrebout Wouter.- S···S and S···P chalcogen bonding in solution : a cryospectroscopic study of the complexes of 2,2,4,4-tetrafluoro-1,3-dithietane w ith dimethyl sulfide and trimethylphosphine
New journal of chemistry - ISSN 1144-0546 - 42:13(2018), p. 10563-10571
Full text (Publisher's DOI): https://doi.org/10.1039/C8NJ01648H
To cite this reference: https://hdl.handle.net/10067/1511030151162165141

S···S and S···P chalcogen bonding in solution: A cryospectroscopic study of the complexes of 2,2,4,4-tetrafluoro-1,3-dithietane with dimethyl sulfide and trimethylphosphine.

Yannick Geboes,[a] Elias De Vos,[a] and Wouter A. Herrebout[a]*

[a] Department of Chemistry, University of Antwerp, Groenenborgerlaan 171, 2020 Antwerp (Belgium), E-mail: wouter.herrebout@uantwerpen.be

Corresponding Author:

W.A. Herrebout: e-mail: wouter.herrebout@uantwerpen.be, +32/3.265.33.73

Keywords: noncovalent interactions, chalcogen bonding, FTIR, cryospectroscopy, liquid krypton

Abstract

In this combined experimental and computational study the complexes formed between 2,2,4,4-tetrafluoro-1,3-dithiethane ($C_2F_4S_2$) and the Lewis bases dimethyl sulfide (DMS) and trimethylphosphine (TMP) are studied using infrared spectroscopy of solutions in liquid krypton. For $C_2F_4S_2$ and DMS, *ab initio* calculations yield two stable chalcogen bonded complex isomers, whereas for $C_2F_4S_2$ and TMP a single chalcogen bonded complex is predicted. In the infrared spectra of solutions containing $C_2F_4S_2$ and DMS, evidence for the presence of two complex bands suggesting the simultaneous occurrence of both calculated complex geometries and the lack of rapid interconversion between them is found for several vibrational modes. The average experimental complexation enthalpy for the 1:1 complexes derived from the van 't Hoff isochores is -12.3(4) kJ mol^{-1}. The calculated values obtained by combining a complete basis set extrapolation approach and corrections for zero-point vibrational, thermal and solvent influences are -17.3 and -15.8 kJ mol^{-1} for the first and second geometry, respectively. For the mixtures of $C_2F_4S_2$ with TMP, single complex bands are found for all vibrational modes, with shifts corresponding well to those of the calculated shifts of the chalcogen bonded complex. The experimental complexation enthalpy for the $C_2F_4S_2$·TMP complex is -13.0(4) kJ mol^{-1}, whereas the calculated value equals -16.1 kJ mol^{-1}.

Introduction

In the last decade halogen bonds, noncovalent interactions formed between positive regions in the electrostatic potential on halogen atoms, often referred to as σ-holes, and electron rich sites, have gained a lot of interest.[1-7] Recently this interest has been expanded towards interactions with group V and group VI elements, giving rise to pnicogen [8-14] and chalcogen bonds.[15-31] Although chalcogen bonds have already shown some promising results for applications in crystallography and catalysis,[28] experimental results characterizing these noncovalent interactions remain scarce.

Triggered by earlier observations suggesting that S⋯O chalcogen bonds might play a role in controlling protein structures [32-34] and in the enzymatic activity of sulfur-containing compounds,[35] we recently initiated a combined experimental and theoretical study focussing on the moderately strong S⋯O chalcogen bonded complex formed between 2,2,4,4-tetrafluoro-1,3-dithiethane ($C_2F_4S_2$) and dimethyl ether (DME).[36] The experimental study involved a vibrational spectroscopic study of the formation of $C_2S_2F_4$·DME dimers in liquid krypton. These measurements typically are performed at moderately low temperatures (varying from 118 to 173 K for liquid krypton) in a solution where the solvent is only weakly interacting with the solutes, thereby creating a pseudo-gas phase environment that is ideally suited to study weak noncovalent interactions.[37] Furthermore, by working at thermodynamic equilibrium and by measuring spectra at various temperatures, thermodynamic properties of the noncovalent interactions, such as the complexation enthalpy, can be determined experimentally.

The choice for $C_2F_4S_2$ as a chalcogen bond donor was based on the observation that, in order to obtain complexes with an appreciable strength, a highly fluorinated molecule is preferred, a strategy that has been followed extensively in studies involving halogen bonding [38-39] and has also been proven to work for chalcogen bonding.[40] The choice for $C_2F_4S_2$ was further motivated by the fact that high purity samples are commercially available, and by the observation that $C_2F_4S_2$ is a rigid molecule with D_{2h} symmetry. As a Lewis base the choice was made for DME, a molecule containing an sp^3 hybridized oxygen atom which has also been used extensively as an oxygen donor in previous cryospectroscopic studies.[41-43] DME had proven to possess no self-associating properties, a phenomenon which is known to limit a thorough analysis [44-45] of the cryospectroscopic data and, in contrast to acetone and ethylene oxide, is known to have a substantial solubility in liquid noble gases. The study of the infrared and Raman spectra on liquid krypton solutions of $C_2F_4S_2$ and DME, not only revealed the presence of complex bands, the shifts being consistent with those of the *ab initio* calculations of the chalcogen bonded complexes, but also allowed the stoichiometry and the complexation enthalpy of the 1:1 complex to be determined, the average value based on temperature ranges in the 120-156 K interval being -13.5(1) kJ mol^{-1}. Comparison with the previously studied halogen bonded complexes between DME and a series of trifluorohalomethanes (CF_3X) [41] shows that this complexation enthalpy lies

between the values of the halogen bonded complex formed with bromotrifluoromethane (ΔH°(LAr) = -10.2(1) kJ mol^{-1}) and the complex formed with trifluoroiodo-methane (ΔH°(LAr) = -15.5(1) kJ mol^{-1}). It is therefore clear that sulphur chalcogen bonds can be comparable in strength with bromine and iodine halogen bonds when the interaction involves the lone pair of an sp^3 hybridized oxygen atom. Obviously, further studies are needed to assess whether this relation holds up when other Lewis bases are used. With the present study we aim at expanding our knowledge of S···S and S···P chalcogen bonded complexes formed by $C_2F_4S_2$. To that end, we have investigated its interaction with dimethyl sulfide (DMS) and trimethylphosphine (TMP), using infrared spectroscopy of liquid noble gas solutions. As before, the experimental studies are supported by *ab initio* calculations, Monte Carlo-Free Energy Perturbation (MC-FEP) simulations and statistical thermodynamics focusing on the geometrical, energetic and spectroscopic properties of the complexes studied. The choice for the Lewis bases dimethyl sulfide and trimethylphosohine is based on earlier observations showing that these Lewis bases can form strong halogen and hydrogen bonded complexes with a variety of electron acceptor molecules including, amongst others, hydrogen bond donors such as halothane [46] and halogen bonded donors such as trifluorohalomethanes.[47] Due to the pronounced electron donating character of the molecules chosen, also no chalcogen or pnicogen type of interactions between the Lewis bases and molecules with electron rich regions are expected, so that interpretation of the data remains rather straightforward.

Experimental

The sample of 2,2,4,4-tetrafluoro-1,3-dithiethane ($C_2F_4S_2$, 97%), was purchased from Alfa Aesar, while samples of dimethyl sulfide (DMS, 99%, anhydrous), trimethylphosphine (TMP, 99%) and trimethylphosphine-d_9 (TMP-d_9, 99 atom% D) were purchased from Sigma-Aldrich. All samples were transferred into glass sample tubes and degassed using a freeze-thaw cycle procedure. The solvent gas krypton was supplied by Air Liquide and had a stated purity of 99.9995%.

The IR spectra were recorded on a Bruker 66v FTIR spectrometer, equipped with a Globar source, a Ge/KBr beam splitter and MCT detector. Measurements were conducted in cells equipped with Si windows and a path length of 10 mm to obtain spectra between 6500 cm^{-1} and 450 cm^{-1}. All interferograms were averaged over 500 scans, Blackman-Harris 3-term apodized and Fourier transformed to yield spectra with a resolution of 0.5 cm^{-1}. Estimated mole fractions of the solutions varied between 1.9×10^{-5} and 1.9×10^{-3} for $C_2F_4S_2$, 5.6×10^{-4} and 1.9×10^{-3} for DMS and 5.6×10^{-4} and 1.9×10^{-3} for TMP. As the experimental setups do not allow for verification of full solubility of the compounds, or verification of the fluid level in the filling tube,[37] exact concentrations are not known. Upon decreasing temperature, for most of the solutions studied, a significant decrease in

intensity is observed for both the monomer bands and the complex bands, suggesting a decreased solubility of the different species involved.

Experimental complexation enthalpies were determined using van 't Hoff plots, based on measurements performed in the 120-156 K temperature interval. The approach typically involves a subtraction procedure in which spectra of monomer solutions, recorded at identical temperatures and similar concentrations, are rescaled and subtracted from the spectrum of the mixture, to obtain a spectrum that solely contains bands due to the complexes present.[37] Subsequently, band intensities for monomers and complexes are integrated numerically. Thermal expansion of the solvent gas during temperature studies was accounted for using the method published by van der Veken.[48] To ensure that no numerical instabilities due to the non-linearity of the MCT detector used could occur during analysis, for all numerical procedures performed, only complex and monomer with an absorbance below 1.0 were considered.

To support the experimental measurements, geometries and harmonic vibrational frequencies of monomers and complexes were obtained from MP2/aug-cc-pVDZ *ab initio* calculations, using Gaussian09.[49] During all calculations, corrections for BSSE were accounted for explicitly by using counterpoise-corrected gradient techniques.[50] Energies at the basis set limit were calculated with Molpro [51] using the extrapolation scheme of Truhlar.[52]

$$E_{CBS}^{HF} = \frac{3^{\alpha}}{3^{\alpha} - 2^{\alpha}} E_3^{HF} - \frac{2^{\alpha}}{3^{\alpha} - 2^{\alpha}} E_2^{HF}$$

$$E_{CBS}^{cor,MP2} = \frac{3^{\beta}}{3^{\beta} - 2^{\beta}} E_3^{cor,MP2} - \frac{2^{\beta}}{3^{\beta} - 2^{\beta}} E_2^{cor,MP2}$$

In these expressions α = 3.4 and β=2.2, [52] while energies with subscript 2 and 3 are calculated using the aug-cc-pVDZ and aug-cc-pVTZ basis sets respectively. An additional correction for higher order correlation effects yielding results of $E_{CBS}^{CCSD(T)}$ quality is made using the method of Jurečka and Hobza.[53]

$$\Delta E^{CCSD(T)} = \left| E^{CCSD(T)} - E^{MP2} \right|_{aug-cc-pVDZ}$$

$$E_{CBS}^{CCSD(T)} = E_{CBS}^{HF} + E_{CBS}^{cor,MP2} + \Delta E^{CCSD(T)}$$

Complexation enthalpies in the vapor phase Δ*H*°(vap,calc) were obtained from the complexation energies Δ*E*(CCSD(T)) by applying a zero-point energy correction and a correction for thermal effects. Correction of the calculated enthalpy values with solvent effects of the liquid noble gas (LNg) yields complexation enthalpies in solution Δ*H*°(LNg,calc), which can be compared with the experimental values Δ*H*°(LNg). Corrections for thermal effects and zero-point vibrational contributions were obtained using statistical thermodynamics, using MP2/aug-cc-pVDZ data. To be

able to correct for solvent influences the Solvation Gibbs energies for monomers and complexes were obtained from Monte Carlo-Free Energy Perturbation (MC-FEP) calculations, using a modified version of BOSS 4.0.[54] To this end, the Gibbs energies of solvation in LKr were calculated at six different temperatures between 119 and 179 K, at a pressure of 28 bar. Subsequently, the enthalpy of solvation $\Delta_{sol}H$ and the entropy of solvation $\Delta_{sol}S$ were extracted using the expressions $\Delta_{sol}S = -(\partial\Delta_{sol}G/\partial T)_P$ and $\Delta_{sol}H = \Delta_{sol}G + T\Delta_{sol}S$.

Ab initio calculations

Inspection of the electrostatic potential on the molecular surface of $C_2F_4S_2$, shown in Figure 1, reveals the presence of four σ-holes, two on both sulphur atoms, which are equivalent due to the D_{2h} symmetry of $C_2F_4S_2$. The presence of multiple σ-holes implies the ability of this molecule to simultaneously undergo interactions with multiple Lewis bases, giving rise to complexes of higher stoichiometry. However, as complexes with such stoichiometry are typically characterized by a significant decrease in entropy, these type complexes are strongly disfavored at equilibrium conditions. Therefore, in this study we have concentrated on the complexes with 1:1 stoichiometry only.

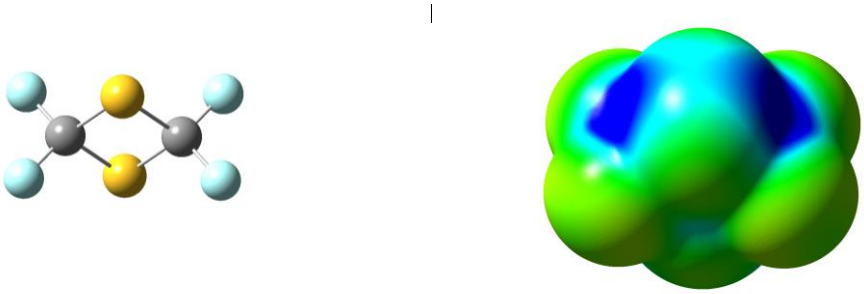

Figure 1: Electrostatic potential of $C_2F_4S_2$ on the molecular surface defined by the 0.001 electrons Bohr^{-3} contour of the electron density, calculated at the MP2/aug-cc-pVDZ level, with positive, neutral and negative regions shown in blue, green and red, respectively.

Geometry optimizations for chalcogen bonded complexes were started at the MP2/aug-cc-pVDZ level using different relative positions of the monomers involved. For $C_2F_4S_2$·DMS, the calculations yielded two different geometries, both having a C_1 symmetry. These complexes will be referred to as the global and local minima in the remainder of this paper. For $C_2F_4S_2$·TMP a single stable complex geometry was obtained. The complex geometries obtained are shown in Figure 2, while the main intermolecular parameters used to define the angular geometry of the complexes and energetics are

summarized in Table 1. The Cartesian coordinates for the monomers and the complexes are summarized in Tables S1 and S2 of the ESI.

The geometries for the S···S and S···P chalcogen bonded complexes all show a strong directionality with a lone pair of the Lewis base oriented directly towards one of the σ-holes in $C_2F_4S_2$. Moreover, for all geometries obtained, close C-H···F contacts, with interatomic distances varying between 2.6 and 2.9 Å can be observed between hydrogen atoms in the Lewis base and one of the fluorine atoms in $C_2F_4S_2$. The appearance of different weak, secondary C-H···F interactions, and the specific orientation of the lone pairs in DMS almost perpendicular towards the plane of the heavy atoms, also explains the occurrence of two different equilibrium geometries for $C_2F_4S_2$·DMS.

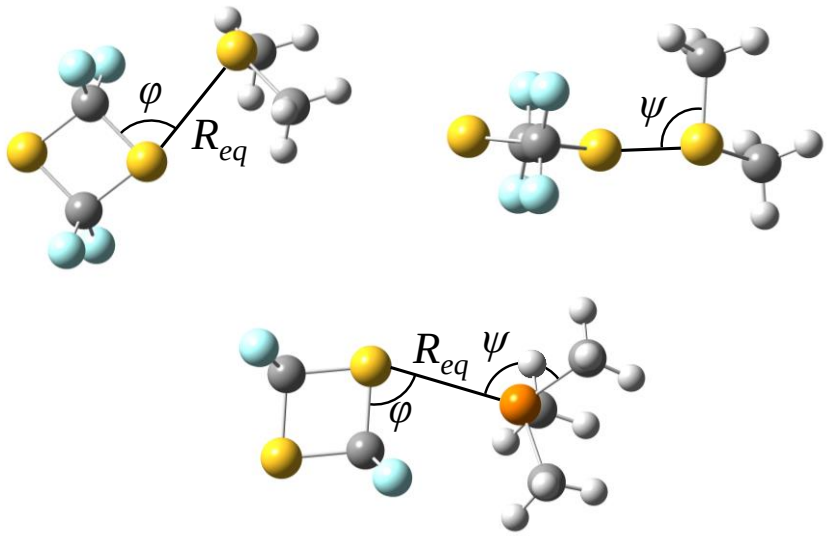

Figure 2: MP2/aug-cc-pVDZ geometries for the chalcogen bonded complexes between $C_2F_4S_2$ and DMS (top) or TMP (bottom).

Table 1: Intermolecular distance R_{eq} (Å) and bond angles (°) from the MP2/aug-cc-pVDZ optimized geometries, MP2/aug-cc-pVDZ Δ*E*(DZ) and CCSD(T)/CBS extrapolated complexation energies Δ*E*(CCSD(T)), calculated vapor phase complexation enthalpies Δ*H*° (vap,calc), the calculated complexation enthalpies in liquid krypton (Δ*H*° (LKr,calc)) and the corresponding experimentally obtained complexation enthalpy (Δ*H*° (LKr)) (kJ mol^{-1}) of the chalcogen bonded complexes between $C_2F_4S_2$ and DMS or TMP.

	DMS		TMP
	Global Minimum	Local Minimum	
Symmetry	C_1	C_1	C_1
R_{eq}=$R_{S\cdots Y}$ [a]	3.19	3.29	3.36
$R_{eq}/\Sigma r_{vdW}$ [b]	0.862	0.888	0.896
φC-S···Y [a]	84.5 / 164.6	82.9 / 163.7	79.3 / 159.8
ψC-Y···S [a]	91.1 / 85.9	93.6 / 115.1	107.8 / 119.7 /126.3
Dihedral [c]	(-)63.2	(-)148.1	72.9 / 60.1

ΔE (DZ)	-22.6	-22.4	-21.3
ΔE (CCSD(T))	-23.9	-23.7	-22.9
$\Delta H°$ (vap,calc)	-21.4	-21.1	-20.4
$\Delta H°$ (LKr,calc)	-17.3	-15.8	-16.1
Experimental			
$\Delta H°$ (LKr)		-12.3(4)	-13.0(4)

[a] Y = S, P
[b] $r_{VdW, S}$ = 1.85 Å; $r_{VdW, P}$ = 1.9 Å
[c] dihedral angle between de C-S axis of $C_2F_4S_2$ and the C-S-C bisector of DMS or the C_3 axis of TMP.

To quantitatively reveal the presence of secondary interactions in the different geometries obtained, for all complexes, the noncovalent interactions (NCI) index was calculated using the MP2 electron densities. The NCI index for the different complexes was then visualized using NCIPLOT.[55-56] Plots of the reduced density gradient versus the electron density multiplied by the sign of the second Hessian eigenvalue and figures showing the gradient isosurfaces are given in Figure 3. Apart from the gradient isosurface belonging to the chalcogen bond itself, which has a blue hue indicating a higher electron density and stronger interaction, also some weaker, green coloured isosurfaces appear for all complexes. Most notable are the additional gradient isosurfaces between the methyl groups of the Lewis bases and the fluorine atoms on $C_2F_4S_2$, indicating the presence of weak stabilizing hydrogen bonds in addition to the chalcogen bond for both complex geometries. For completeness, for all complexes studied, bond critical points, ring critical points and bond paths obtained from an Atoms In Molecules (AIM) approach [57-59] using the MP2 electron densities are added to Figure S1 of the ESI. It can be seen that for the first dimethyl sulfide containing complex, no bond critical points or bond paths illustrating secondary interactions are found. In contrast, for second type of complex, a more complex pattern including two additional bond critical points and two additional bond paths connecting the hydrogen atoms in the DMS moiety and a fluorine atom in $C_2F_4S_2$ are observed. Finally, also for the complex with TMP, two different types of interactions can be envisaged. The first interaction involves the phosphorus atom in TMP and a sulphur atom in $C_2F_4S_2$ and can be related to the chalcogen bond present. The secondary, most probably much weaker, interaction involves a fluorine atom in $C_2F_4S_2$ and the phosphorus atom in TMP, and might originate from a secondary but weak F…P pnicogen bond.

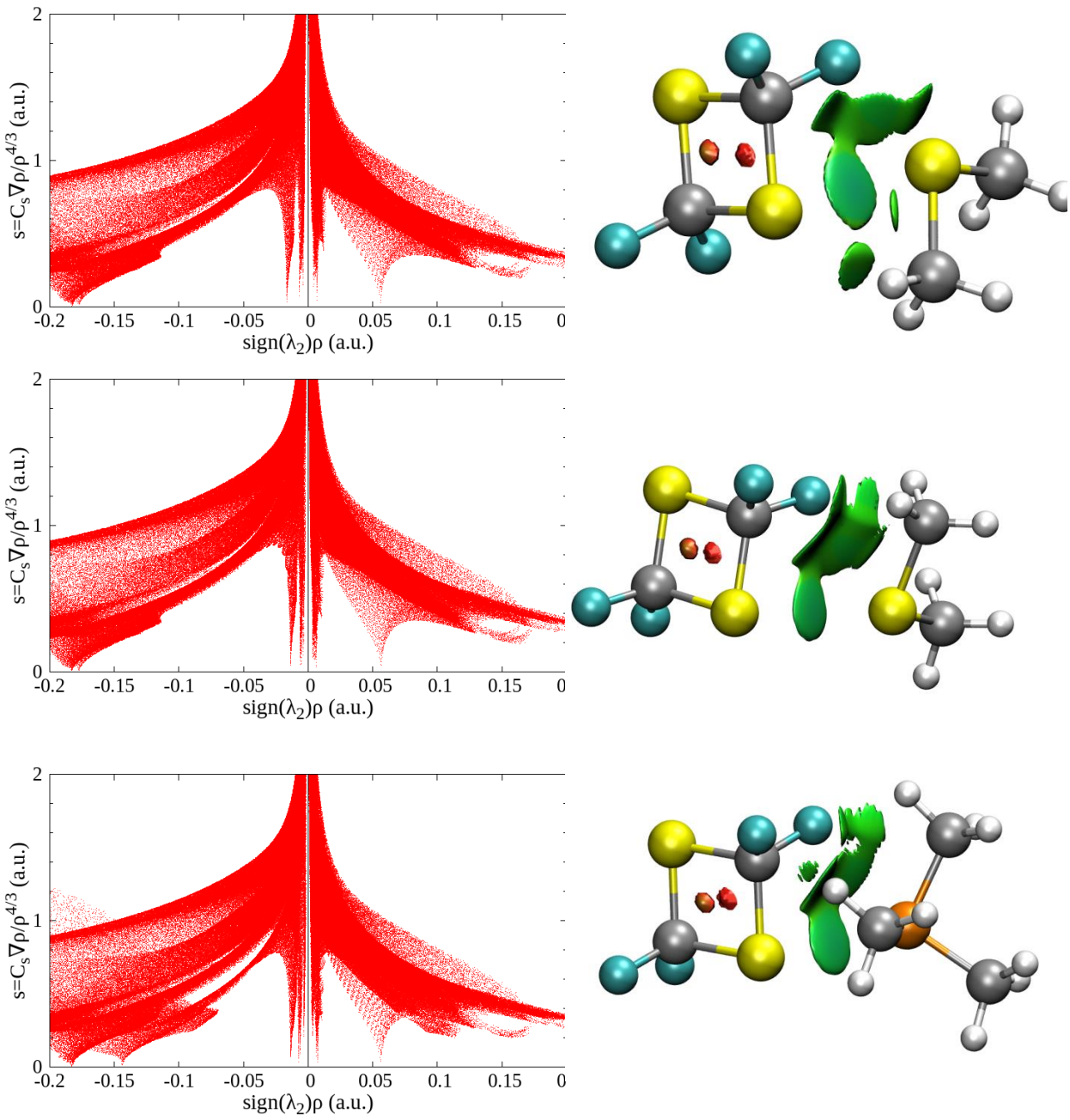

Figure 3: Plots of the reduced density gradient versus the electron density multiplied by the sign of the second Hessian eigenvalue (left) and gradient isosurfaces (s = 0.5 a.u., right) for the chalcogen bonded complex between $C_2F_4S_2$ and DMS at the global minimum (top) and the local minimum (middle), and for the chalcogen bonded complex between $C_2F_4S_2$ and TMP (bottom).

It is interesting to note that for the S···O chalcogen bonded complex with dimethyl ether, $C_2F_4S_2$·DME, complexes with C_s symmetry were found with and without secondary C-H···F interactions, the MP2/aug-cc-pVDZ complexation energies being -23.2 and -22.2 kJ mol^{-1}, respectively. Such pattern clearly is not observed for the S···S chalcogen bonded complex

$C_2F_4S_2$·DMS studied here. We believe that these differences are related to the more diffuse character and the different positioning of the lone pairs in the DMS compared to those in DME. Another difference between both type of complexes observed is related to the energy barrier separating the different equilibrium geometries. For $C_2F_4S_2$·DME, a transition state search between the different complex geometries using the Synchronous Transit-Guided Quasi-Newton method, yielded a transition state yielded a transition state with a single imaginary frequency of -42 cm^{-1}, a mere 0.7 kJ mol^{-1} higher in energy than the less stable complex geometry. Therefore, rapid interconversion between both complex geometries and an averaged structure was expected to be observed during the experimental measurements. A similar transition state search between the different complex geometries was also attempted for $C_2F_4S_2$·DMS, but yielded no results as the molecules separated completely during all calculations performed. This suggests the presence of a high energy barrier, limiting the rapid interconversion between the local and global minima in $C_2F_4S_2$·DMS. This conclusion is in line with the experimental observations (*vide infra*) suggesting that for the $C_2F_4S_2$·DME complexes, only single bands related to the averaged geometry are observed, whereas for some of the vibrational modes in $C_2F_4S_2$·DMS a doublet consisting of two, slightly shifted, transitions can be identified that could be assigned to the two different types of complexes present.

Inspection of the complexation energies and the corresponding values for the complexation enthalpies in the vapor phase and in the solution, shows that the values obtained for the S···S chalcogen bonded and those obtained for S···P chalcogen bonded complexes are very similar, typical variations being in the order of 4 to 7% only. The values also compare well with the data for $C_2F_4S_2$·DME summarized in Table S3 of the ESI, suggesting that for S···X (X = O, S and P) chalcogen bonding, the intrinsic strength of the interaction hardly changes when passing from oxygen to sulphur and phosphorus. The large similarities observed suggest that for all complexes studied, the chalcogen bond type of interaction dominates the intermolecular interaction. The similarities also are illustrated by the results of Natural Bond Orbital (NBO) analyses [60] suggesting that in the complexes with DMS and TMP, a similar electron transfer from a lone pair in the Lewis base to one of the σ-holes in $C_2F_4S_2$ is observed, the values based on the MP2/aug-cc-pVDZ electron density being –0.041e and –0.031e for the complexes with DMS, and –0.033e for the complex with TMP. For comparison, also the values for the two types of complexes with DME reported before were calculated, the results being -0.017e and -0.022e.

The MP2/aug-cc-pVDZ harmonic vibrational frequencies and infrared intensities for the monomers and for the 1:1 complexes have been collected in Tables S4 to S6 of the ESI. It is worth noting that for the complexes with DMS, the complexation shifts for the global minimum in general are slightly smaller than those obtained for the local minimum, the shifts varying between -6.2 and +5.1 cm^{-1}, and between -11.1 and +9.5 cm^{-1}. The predicted complexation shifts, therefore, are not directly related to the strength of the interaction. The complexation shifts for the complex with TMP vary from -13.6 to

+7.0 cm^{-1}, and are in line with the above statement. For all geometries, the complexation shifts also are significantly larger for the vibrational modes of $C_2F_4S_2$, typical examples being ν_8 (B_{1u}), ν_{11} (B_{2g}) and ν_{18} (B_{3u}). For the modes of A_g, A_u, B_{1g}, B_{2g}, and B_{3g} modes that are infrared forbidden in the monomer, complexation with DMS and TMP leads to a substantial induced infrared intensity that could allow these modes to be identified in the experimental spectra.

Vibrational Spectra

The assignment of the $C_2F_4S_2$ vibrational modes has been discussed in detail before,[36] while the assignments of DMS and TMP are readily available in literature.[46-47] In order to aid assignments of the complex bands observed, experimental observations were compared with the calculated frequencies, complexation shifts and infrared intensities in Tables S4 to S6.

Experimental evidence for the formation of complexes is typically obtained by carefully comparing spectra of monomers and mixtures and by the observation of new bands appearing upon mixing. Moreover, more accurate data is obtained using so-called subtraction procedures in which spectra of the monomers recorded under identical circumstances, including e.g. the exact same temperature, are multiplied by a scaling factor and subsequently subtracted from the spectrum of the mixture.[37] The value of this scaling factor is such that, after subtraction, no features due to the monomers are withheld and that the remaining spectrum thus solely contains bands assigned to the complexes formed. The subtraction method is strongly preferred for cases in which the complexation shifts between monomer and complex are small, and for which the resulting bands due to monomers and complexes largely overlap with each other, as is the case for the mixtures studied here.

Solutions containing $C_2F_4S_2$ and dimethyl sulfide

Subtraction of monomer spectra from spectra of the mixtures, leads to multiple spectral regions where monomer and complex bands can be identified, a selection of them is shown in Figure 4. Most notable are the -3.8 cm^{-1} redshifted band for the $C_2F_4S_2$ ν_{16} mode and -5.9 cm^{-1} redshifted band for the $C_2F_4S_2$ ν_8, shown in Panel 4A. Both complexation shifts are in good agreement with the calculated redshifts for the respective vibrational modes of -5.9 and -6.2 cm^{-1} obtained for the global minimum, albeit that a substantial broadening in the complex is observed for the ν_{16} band. The broadening, most probably, is caused by the appearance of two absorption bands with a similar intensity slightly shifted from each other. A similar, more expressed, pattern confirming this interpretation is also observed for the $C_2F_4S_2$ ν_{13} modes, shown in Panel 4B, Upon subtraction, an asymmetric redshifted band profile is observed. Analysis of the band profile suggests that the spectral pattern involves two contributions redshifted from the monomer band, by -2.7 cm^{-1} and -1.7 cm^{-1}. The appearance of two spectral transitions for the $C_2F_4S_2$ ν_{13} and ν_{16} modes is in line with the above suggestion that in cryosolutions two different types

of S···S complexes can be formed simultaneously and that both complexes can be detected separately. This interpretation is further supported by the observation of -5.3 cm^{-1} and -3.3 cm^{-1} redshifted bands for the $C_2F_4S_2$ ν_{13} mode, which can be assigned to the global minimum and local minimum, respectively, using the *ab initio* calculated complexation shifts. Other vibrational modes worth mentioning include the $C_2F_4S_2$ ν_{17} mode shown in Panel 4C ($\Delta\nu_{exp}$ = -1.8 cm^{-1}, $\Delta\nu_{calc,global}$ = -2.4 cm^{-1} and $\Delta\nu_{calc,local}$ = -2.3 cm^{-1}) and the DMS ν_{14} mode ($\Delta\nu_{exp}$ = 2.4 cm^{-1}, $\Delta\nu_{calc,global}$ = 2.1 cm^{-1} and $\Delta\nu_{calc,local}$ = 3.0 cm^{-1}). An additional weak band due to the complex is also observed at 832.7 cm^{-1}. As no other IR active vibrational modes are expected to appear in this spectral region, and supported by the calculated frequencies and infrared intensities in Table S3, this complex band is assigned to $C_2F_4S_2$ ν_6 mode. This band is infrared inactive for monomer $C_2F_4S_2$, but is IR active in the complexes, the predicted infrared intensity for the global and the local minimum being 6.4 and 6.2 km $mol^{-1,}$ respectively.

For completeness, an overview of all infrared active transitions of $C_2F_4S_2$, DMS and their complexes, including experimental and calculated complexation shifts, are listed in Table 2.

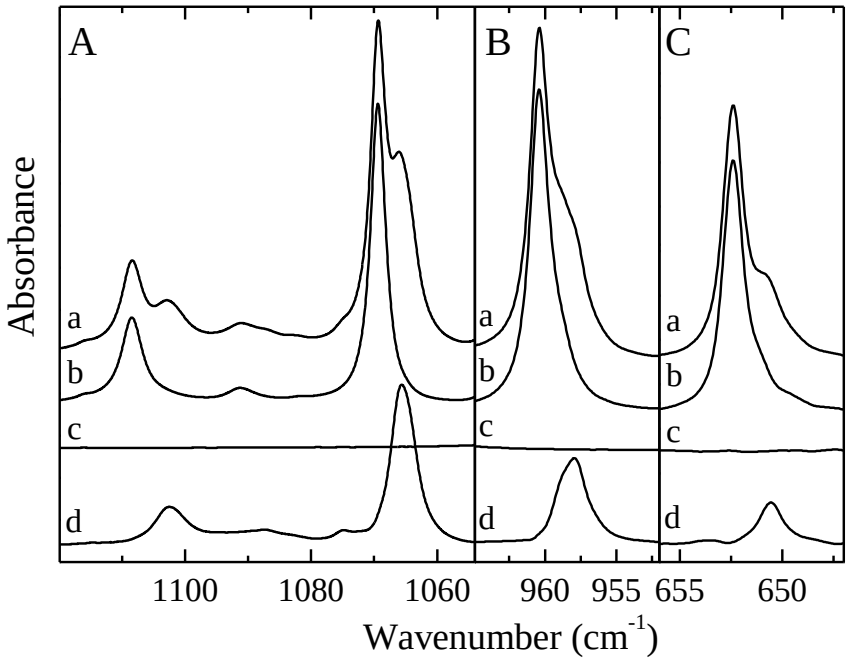

Figure 4: Infrared spectra of selected spectral regions for the mixtures of $C_2F_4S_2$ with DMS dissolved in LKr at 133 K. In each panel, trace *a* represents the mixed solution, while traces *b* and *c* show the rescaled spectra of the solutions containing only $C_2F_4S_2$ or DMS, respectively. Trace *d* represents the spectrum of the complex which is obtained by subtracting the rescaled traces *b* and *c* from trace *a*. Estimated mole fractions of the solutions of the mixtures are 9.4×10^{-5} for $C_2F_4S_2$ and 4.7×10^{-4} for DMS in panel A and 1.9×10^{-3} for $C_2F_4S_2$ and 5.6×10^{-4} for DMS in panels B and C.

Table 2: Experimental vibrational frequencies for the monomer and complexes, as well as experimental complexation shifts ($\Delta\nu_{exp}$) and MP2/aug-cc-pVDZ calculated complexation shifts ($\Delta\nu_{calc}$), in cm^{-1}, for the chalcogen bonded complex of $C_2F_4S_2$ with DMS dissolved in LKr at 133 K.

	Assignment	$\nu_{monomer}$	$\nu_{complex}$	$\Delta\nu_{exp}$	$\Delta\nu_{calc,global}$	$\Delta\nu_{calc,local}$
$C_2F_4S_2$	$\nu_3 + \nu_{17}$	1165.5	1163.6	-1.9	-3.7	-3.1
	$\nu_6 + \nu_{14}$	1165.5	1163.6	-1.9	-3.7	-1.5
	$\nu_2 + \nu_{18}$	1115.9	-		-3.8	-3.8
	ν_8	1108.4	1102.5	-5.9	-6.2	-11.1
	$\nu_2 + \nu_9$	1091.2	1087.3	-3.9	-1.1	-1.5
	ν_{11}	-	-		-5.5	-9.7
	$\nu_7 + \nu_{17}$	1081.6	-		-0.6	-1.0
	$\nu_2 + \nu_7$	-	1074.8		-1.1	-2.0
	ν_{16}	1069.4	1065.6	-3.8	-5.9	-9.7
	ν_{16} (^{13}C)	1053.1	1049.7	-3.4	-5.9	-9.7
	$\nu_{12} + \nu_{17}$	1029.9	1032.0	2.1	1.6	1.6
	ν_{13}	960.4	958.7	-1.7		-3.3
	“	“	957.7	-2.7	-5.3	
	ν_{13} (^{13}C)	947.5	-		-5.3	-3.3
	ν_6	835.5 [a]	832.7	-2.8	-4.3	-2.2
	ν_{17}	652.4	650.6	-1.8	-2.4	-2.3
	ν_{18}	450.1	-		-0.9	-0.5
DMS	ν_1	2991.6	2995.2	3.6	2.0	2.0
	ν_{16}	2991.6	2995.2	3.6	5.1	4.6
	ν_{12}	2965.1	2970.6	5.5	-0.4	9.5
	ν_{17}	2920.6	2920.6	0.0	-1.6	4.2
	ν_2	2917.1	2916.0	-1.1	-2.6	4.2
		2883.5	2880.7	-2.8		
		2864.4	2863.0	-1.4		
		2856.3	2854.2	-2.1		
	$2\nu_9$	2838.2	2836.4	-1.8	-5.0	-3.6
	ν_3	1444.9	1442.5	-2.4	-2.5	-1.0
	ν_{18}	1438.4	1436.7	-1.7	-3.0	-1.6
	ν_{13}	1432.9	1432.0	-0.9	-2.3	-1.6
	ν_{19}	1310.3	1311.3	1.0	-0.4	-0.9
	ν_5	1030.6	1032.0	1.4	0.6	0.6
	ν_{14}	973.1	975.5	2.4	2.1	3.0
	ν_{20}	902.0	-		2.4	2.5
	ν_6	696.1	-		-1.7	-2.5

[a] Wavenumber determined from a Raman measurement in LKr at 147 K.[36]

Solutions containing $C_2F_4S_2$ and trimethylphosphine

In Figure 5, typical spectra obtained for mixtures of $C_2F_4S_2$ and TMP are compared with the rescaled monomer spectra and with the complex spectra obtained using the subtraction procedure. An overview of the observed complexation shifts in the interacting moieties and their assignments are collected in Table 3.

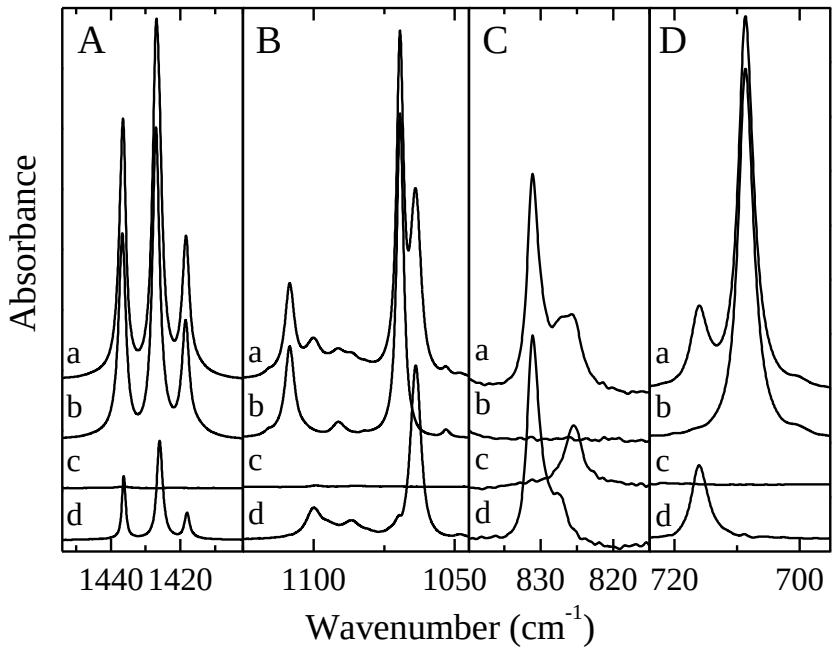

Figure 5: Infrared spectra of selected spectral regions for the mixtures of $C_2F_4S_2$ with TMP dissolved in LKr at 133 K. In each panel, trace *a* represents the mixed solution, while traces *b* and *c* show the rescaled spectra of the solutions containing only $C_2F_4S_2$ or TMP, respectively. Trace *d* represents the spectrum of the complex which is obtained by subtracting the rescaled traces *b* and *c* from trace *a*. Estimated mole fractions of the solutions of the mixtures are 3.8×10^{-4} for $C_2F_4S_2$ and 5.6×10^{-4} for TMP in panels A, C and D and 2.8×10^{-5} for $C_2F_4S_2$ and 1.1×10^{-3} for TMP in panel B.

Table 3: Experimental vibrational frequencies for the monomer and complexes, as well as experimental complexation shifts ($\Delta\nu_{exp}$) and MP2/aug-cc-pVDZ calculated complexation shifts ($\Delta\nu_{calc}$), in cm^{-1}, for the chalcogen bonded complex of $C_2F_4S_2$ with TMP dissolved in LKr at 133 K.

	Assignment	$\nu_{monomer}$	$\nu_{complex}$	$\Delta\nu_{exp}$	$\Delta\nu_{calc}$
$C_2F_4S_2$	$\nu_3 + \nu_{17}$	1165.5	1158.3	-7.2	-5.6
	$\nu_6 + \nu_{14}$	1165.5	1158.3	-7.2	-3.5
	$\nu_2 + \nu_{18}$	1115.9	-		-5.7
	ν_8	1108.4	1100.0	-8.4	-13.6
	$\nu_2 + \nu_9$	1091.2	1086.4	-4.8	-2.8
	ν_{11}	-			-13.6
	$\nu_7 + \nu_{17}$	1081.6	-		-2.6
	$\nu_2 + \nu_7$	-			-3.5
	ν_{16}	1069.4	1063.8	-5.6	-10.4
	ν_{16} (^{13}C)	1053.1	1048.2	-4.9	-10.4
	$\nu_{12} + \nu_{17}$	1029.9	1030.7	0.8	0.4
	ν_{13}	960.4	957.3	-3.1	-3.2
	ν_{13} (^{13}C)	947.5	-		-3.2
	ν_6	835.5 [a]	831.1	-4.4	-3.1
	ν_{17}	652.4	649.0	-3.4	-3.5
	ν_{18}	450.1	448.6	-1.5	-1.4

TMP	ν_{12}	2972.0	2976.8	4.8	4.4
	ν_1	2957.9	2962.5	4.6	3.5
	ν_{13}	2957.9	2962.5	4.6	4.2
	ν_2	2897.3	2900.3	3.0	3.1
	ν_{14}	2897.3	2900.3	3.0	3.1
	ν_3	1436.7	1436.3	-0.4	-1.3
	ν_{15}	1427.0	1426.0	-1.0	-1.1
	ν_{16}	1418.5	1418.1	-0.4	-1.2
	$\nu_6 + \nu_{20}$	1359.2	1369.6	10.4	9.0
	$2\nu_6$	1310.9	1315.2	4.3	3.9
	ν_4	1295.1	1297.9	2.8	0.3
	ν_{17}	1278.8	1281.0	2.2	0.5
	ν_5	948.9	948.7	-0.2	-0.7
	ν_{18}	937.6	940.1	2.5	2.5
	ν_{19}	825.4	828.4	3.0	1.8
	ν_{20}	708.7	716.1	7.4	7.0
	ν_6	653.9	656.6	2.7	1.9

[a] Wavenumber determined from a Raman measurement in LKr at 147 K.[36]

In agreement with the results for DMS, bands illustrating complex formation between $C_2F_4S_2$ and TMP are observed for the $C_2F_4S_2$ ν_{16} and ν_8 modes shown in Panel 5B. The redshifts for these modes, -5.6 and -8.4 cm^{-1}, again are in good agreement with the calculated frequencies, the predicted complexation shifts being -10.4 cm^{-1} and -13.6 cm^{-1}, respectively. A strong feature, blue shifted from the monomer band by +7.4 cm^{-1}, is also observed for the TMP ν_{20} mode shown in Panel 5D. Also here, a good agreement is found between the experimental complexation shift and the theoretical value of +7.0 cm^{-1}. Also for the ν_3, ν_{15} and ν_{16} vibrational modes in TMP, shown in Panel 5A, complex bands redshifted from these monomer transitions by -0.4 cm^{-1}, -1.0 cm^{-1} and -0.4 cm^{-1}, respectively, are observed. Although relatively small, these values also agree favorably with the predicted shifts of -1.3, -1.1 and-1.2 cm^{-1} respectively.

As shown in panel 5C, also for solutions containing $C_2F_4S_2$ and TMP a complex band related to the $C_2F_4S_2$ ν_6 mode becoming IR active upon complexation can be identified, at 831.1 cm^{-1}. It should be noted that, in contrast to the solutions containing DMS, this spectral region also contains a band due to the ν_{19} mode of TMP as well as its complex band. To confirm that the most intense complex band at 831.1 cm^{-1} is indeed related to the $C_2F_4S_2$ ν_6 mode, an additional measurement was performed using the fully deuterated TMP-d_9 as a Lewis base, which has no vibrational modes in this spectral region. The spectra obtained for this species are summarized in Figure S2 of the ESI. It can be seen that for these solutions, the complex band at 831.1 cm^{-1} is retained, while the band at 828.4 cm^{-1} tentatively assigned to the ν_{19} TMP mode in the complex is no longer observed in the spectra of the solutions containing TMP-d_9.

Experimental Complexation Enthalpies

The standard complexation enthalpies for the complexes in LKr were derived by using the van ’t Hoff equation. This equation establishes a linear relation with a slope related to $\Delta H°(\mathrm{LKr})/R$, between the reciprocal temperature and the logarithm of the intensity product I_{complex} / ($I_{C_2F_4S_2} \times I_{\mathrm{LB}}$), with I_{complex}, $I_{C_2F_4S_2}$and I_{LB} the intensities of a complex, a $C_2F_4S_2$ monomer and a Lewis base monomer band, respectively. The absorptions of several bands and mixtures were used of spectra recorded between 121 and 155 K. An overview of various temperature studies, the concentrations of the monomers used, and the numerical approaches used to determine the respective integrated intensities are summarized in Table S7 of the ESI for $C_2F_4S_2$·DMS and Table S8 for $C_2F_4S_2$·TMP. For all temperature studies performed, the standard complexation enthalpies were derived from the slopes of the regression lines and by using an additional correction factor for the thermal expansion of the solvent. For the $C_2F_4S_2$·TMP complex six complexation enthalpies were obtained, varying between -12.5 and -13.8 kJ mol^{-1}, the average complexation enthalpy being -13.0(4) kJ mol^{-1}. For the complexes with DMS, seven complexation enthalpies were determined between -11.7 and -13.0 kJ mol^{-1}, the average being -12.3(4) kJ mol^{-1}.

Discussion

Apart from the spectral features assigned to the monomers involved, in the infrared spectra of the solutions in liquid krypton containing mixtures of $C_2F_4S_2$ and DMS and of $C_2F_4S_2$ and TMP, separate features due to 1:1 complexes are observed. Hence, for both Lewis bases, direct spectroscopic evidence for the co-existence of monomer and complexes, each with a separate spectrum, is found. The study of the binary complexes between $C_2F_4S_2$ and DMS and between $C_2F_4S_2$ and TMP reported here, clearly is one of the first studies reporting the existence of S···S and S···P chalcogen bonded molecular complexes in solution. Moreover, due to the inert nature of the solvent used, the intrinsic properties of the complex are observed nearly free of any solvent perturbations.

Ab initio calculations for the complex with DMS yielded two stable chalcogen bonded complex isomers, which are distinguished by the presence of different F···H secondary interactions. In agreement with the calculated frequencies and infrared intensities for both types of complex, and in agreement with the observation that no interconversion pathway allowing a rapid interconversion between the minima is found, two separate complex bands suggesting the simultaneous occurrence of the two types of complexes are observed in some spectral regions. These results for DMS contrast with the data for the complexes with DME, illustrating that for this complex, a low-energy barrier allowing a rapid interconversion between different minima is present. The differences between both Lewis bases, most probably, are related to the differences in intermolecular distance due to the size of

the oxygen and the sulphur atom present, and to the different orientation of their electron lone pairs with respect to the C_2 symmetry axis. As all splittings suggesting the simultaneously occurrence of the two types of complexes are very small, and thus lead to strongly overlapping features in the spectra, all attempts to reliably determine the integrated intensities of the separate underlying transitions were deemed unsuccessful. Therefore, during further analysis, for the complexes with DMS only an average value for the complexation energy of the complex was derived.

The average experimental complexation enthalpies of -12.3(4) kJ mol^{-1} for $C_2F_4S_2$·DMS and -13.0(4) kJ mol^{-1} for $C_2F_4S_2$·TMP are is in line with the calculated complexation solution phase enthalpies of -17.3, -15.8 and -16.1 kJ mol^{-1}, obtained for the global and local minimum of $C_2F_4S_2$·DMS. Moreover, a good agreement is found with the experimental and theoretical values reported for the S···O chalcogen bonded complex.[36] The experimental values, therefore, are in line with the predicted trends suggesting that for S···X chalcogen bonding, the strength of the interaction hardly changes when passing from oxygen to sulphur and phosphorus. Comparison of the data obtained for the various complexes with $C_2F_4S_2$ and for the complexes of DME and DMS with the trifluorohalomethanes CF_3X (X = Cl, Br, and I) further shows that sulphur based chalcogen bonds are comparable in strength with bromine and iodine halogen bonds. The results reported here therefore further illustrate the earlier observation [36] that chalcogen bonds hold great potential to form stronger noncovalent interactions than halogen bonds involving halogens from the same period of the periodic table.

Conclusions

Ab initio calculations at the MP2/aug-cc-pVDZ level of theory yielded two stable chalcogen bonded complexes between $C_2F_4S_2$ and DMS and one stable chalcogen bonded complex between $C_2F_4S_2$ and TMP. Analysis of the complexes with NCIPlot and Atoms in Molecules revealed that for DMS the difference between both isomers is related to occurrence of different secondary F···H interactions.

Using infrared spectroscopy on liquid krypton solutions of $C_2F_4S_2$ and DMS and of $C_2F_4S_2$ and TMP, the presence of complex bands is revealed, the shifts being consistent with those of the *ab initio* calculations of the chalcogen bonded complexes. In agreement with the calculated frequencies and infrared intensities for both types of complex, and with the observation that no interconversion path way allowing a rapid interconversion between the minima is found, two separate complex bands suggesting the simultaneous occurrence of the two type of complexes are observed in some spectral regions. These results for DMS contrast with the data for the complexes with DME, illustrating that for this complex, a low-energy barrier allowing a rapid interconversion between the different minima is present.

An average experimental complex enthalpy of -12.3(4) kJ mol^{-1} for $C_2F_4S_2$·DMS and -13.0(4) kJ mol^{-1} for $C_2F_4S_2$·TMP is found by analyzing van 't Hoff plots of measurements in liquid krypton in the 121-155 K temperature interval. This value also agrees favorably with the calculated complexation enthalpy values of -16.6 and -15.2 kJ mol^{-1} for the chalcogen bonded complexes. Moreover, a good agreement is found with the experimental and theoretical values reported for the S···O chalcogen bonded complex.[36] The experimental values, therefore, are in line with the predicted trends suggesting that for S···X chalcogen bonding, the strength of the interaction hardly changes when passing from oxygen to sulphur and phosphorus. It is also concluded that sulphur based chalcogen bonds are comparable in strength with comparable bromine and iodine halogen bonds. The results reported here therefore again show chalcogen bonds hold great potential to form stronger noncovalent interactions than halogen bonds involving halogens from the same period of the periodic table.

Acknowledgements

Y.G. and W.H. acknowledges financial support through FWO-Vlaanderen and the Special Research Fund BOF (UA). The Hercules foundation and the VSC are thanked for generously providing the required CPU resources.

References

1. P. Metrangolo, J.S. Murray, T. Pilati, P. Politzer, G. Resnati, and G. Terraneo, *Crystal Growth & Design*, 2011, **11**, 4238.

2. J. Kemsley, *Chem. Eng. News Archive*, 2012, **90**, 36.

3. L.C. Gilday, S.W. Robinson, T.A. Barendt, M.J. Langton, B.R. Mullaney, and P.D. Beer, *Chem. Rev.*, 2015, **115**, 7118.

4. F. Biedermann and H.-J. Schneider, *Chem. Rev.*, 2016, **116**, 5216.

5. G.Cavallo, P. Metrangolo, R. Milani, T. Pilati, A. Priimagi, G. Resnati, and G. Terraneo, *Chem. Rev.*, 2016, **116** , 2478.

6. M.H. Kolář and P. Hobza, *Chem. Rev.*, **2016**, **116**, 5155.

7. P. Molina, F. Zapata, and A. Caballero, *Chem. Rev.*, 2017, **117**, 9907.

8. I. Alkorta, G. Sánchez-Sanz, J. Elguero and J.E. Del Bene, *J. Chem. Theory Comput.*, 2012, **8**, 2320.

9. S. Scheiner, *Acc. Chem. Res.*, 2013, **46**, 280.

10. D. Setiawan, E. Kraka, and D. Cremer, *J. Phys. Chem. A*, 2015, **119**, 1642.

11. H. Zhuo, Q. Li, W. Li and J. Cheng, *New J. Chem.*, 2015, **39**, 2067.

12. S. Sarkar, M.S. Pavan and T. N. Guru Row, *Phys. Chem. Chem. Phys.*, 2015,**17**, 2330.

13. I. Alkorta, J. Elguero and J.E. Del Bene, *Phys. Chem. Chem. Phys.*, 2016,**18**, 32593.
14. J. Schmauck and M. Breugst , *Org. Biomol. Chem.***,** 2017**,15,** 8037.
15. A. Bauzá, D. Quiñonero, P.M. Deyà and A. Frontera, *CrystEngComm***,** 2013,**15**, 3137.
16. V.dP. N. Nziko and S. Scheiner, *J. Phys. Chem. A*, 2014, **118**, 10849.
17. U. Adhikari and S. Scheiner, *J. Phys. Chem. A*, 2014, **118**, 3183.
18. S. Scheiner, *J. Phys. Chem. A*, 2015**, 119,** 9189.
19. V.dP. N. Nziko and S. Scheiner, *J. Phys. Chem. A*, 2015, **119**, 5889.
20. V.dP. N. Nziko and S. Scheiner, *J. Org. Chem.*, 2015, **80**, 2356.
21. L.M. Azofra, I. Alkorta, and S. Scheiner, *J. Phys. Chem. A*, 2015, **119**, 535.
22. G.E. Garrett, G. L. Gibson, R.N. Straus, D.S. Seferos, and M.S. Taylor, *J. Am. Chem. Soc.* 2015, **137**, 4126.
23. R. Shukla and D. Chopra , *Phys. Chem. Chem. Phys.*, 2016, **18**, 13820.
24. I. Khan, P. Panini, S. Ud-Din Khan, U. Ali Rana, H.a Andleeb, D. Chopra, S. Hameed, and J. Simpson, *Crystal Growth & Design*, 2016**, 16**, 1371.
25. R.J. Fick, G.M. Kroner, B. Nepal, R.Magnani, S. Horowitz, R.L. Houtz, S. Scheiner, and R.C. Trievel, *ACS Chem. Biol.*, 2016**, 11**, 748.
26. A.C. Legon, *Phys. Chem. Chem. Phys***.**, 2017, **19**, 14884.
27. L. Brammer, *Faraday Discuss***.**, 2017, **203**, 485.
28. K.T. Mahmudov, M.N. Kopylovich, M. Fátima C. Guedes da Silvaa and A.J. L.Pombeiro, *Dalton Trans***.**, 2017, **46**, 10121.
29. D.J. Pascoe, K.B. Ling, and S.L. Cockroft, *J. Am. Chem. Soc.*, 2017, **139**, 15160.
30. S. Benz, J. López-Andarias, J. Mareda, N. Sakai, S. Matile, *Angew. Chem. Int. Ed.*, 2017, **56**, 812.
31. V. Oliveira, D. Cremer, and E. Kraka , *J. Phys. Chem. A*, 2017, **121**, 6845
32. M. Iwaoka, S. Takemoto, and S. Tomoda, *J. Am. Chem. Soc.* 2002, **12**4, 10613.
33.M. Iwaoka and N.Isozumi, *Molecules*, 2012, **17**, 7266.
34. M. Iwaoka, S. Takemoto, O. Mai, and S. Tomoda, *Chem. Lett.* 2001, **30**, 132.
35. J.C. Taylor, G.D. Markham, *J. Biol. Chem.* 1999, **274**, 32909.
36. Y. Geboes, F. De Vleeschouwer, F. De Proft, W. A. Herrebout, *Chem. Eur. J.*, 2017, **23**, 17384.
37. W. A. Herrebout, *Top. Curr. Chem.*, 2015, **358**, 79.
38. G. Valerio, G. Raos, S.V. Meille, P. Metrangolo, G. Resnati, *J. Phys. Chem. A* 2000, **104**, 1617.
39. K.E. Riley, J.S. Murray, J. Fanfrlik, J. Rezac, R.J. Sola, M.C. Concha, F.M. Ramos, and P. Politzer, *J. Mol. Model.*, 2011, **17**, 3309.
40. R.Shukla and D Chopra, *J. Chem. Sci.* 2016, **128**, 1589.
41. D. Hauchecorne, R. Szostak, W.A Herrebout, and B.J. van der Veken, *ChemPhysChem* 2009, **10**, 2105.
42. Y. Geboes, N. Nagels, B. Pinter, F. De Proft, and W.A. Herrebout, *J. Phys. Chem. A*, 2015, **119**, 2502.
43. Y. Geboes, F. De Proft, and W.A. Herrebout, *Chem. Phys*. 2016, **476**, 1.

44. L.I. De Beuckeleer, and W.A. Herrebout, *J. Phys. Chem. A*, 2016, **120**, 884.
45. L.I. De Beuckeleer, and W.A. Herrebout, *Spectrochim. Acta Part A*, 2017, **171**, 60.
46. B. Michielsen, C.Verlackt, B. van der Veken, and W. Herrebout, *J. Mol. Struct.*, 2012, **1023**, 90.
47. D. Hauchecorne, A. Moiana, B.J. van der Veken, and W.A. Herrebout. *Phys. Chem. Chem. Phys.*, 2011, **13**, 10204.
48. B.J. van der Veken, *J. Phys. Chem.*, 1996, **100**, 17436.
49. M.J. Frisch, et al., Gaussian 09, Revision D.01, Wallingford, CT, USA, 2009.
50. P. Salvador, and M.M. Szczesniak, *J. Chem. Phys.*, *2003*, **118**, 537.
51. H.-J. Werner, et al., MOLPRO, version 2012.1, A Package of Ab Initio Programs, 2012.
52. D.G. Truhlar, *Chem. Phys. Lett*., 1998, **294**, 45.
53. P. Jurečka, P. Hobza, *J. Am. Chem. Soc.*, 2003, **125**, 15608.
54. W.L. Jorgensen, BOSS - Biochemical and Organic Simulation System, John Wiley & Sons Ltd., New York, NY, USA, 1998.
55. E.R. Johnson, S. Keinan, P. Mori-Sánchez, J. Contreras-García, A.J. Cohen, and W. Yang, *J. Am. Chem. Soc.*, 2010, **132**, 6498.
56. J. Contreras-García, E.R. Johnson, S. Keinan, R. Chaudret, J.-P. Piquemal, D.N. Beratan, and W. Yang, *J. Chem. Theor. Comp*., 2011, **7**, 625.

S···S and S···P chalcogen bonding in solution: A cryospectroscopic study of the complexes of 2,2,4,4-tetrafluoro-1,3-dithietane with dimethyl sulfide and trimethylphosphine.

Yannick Geboes,[a] Elias De Vos,[a] and Wouter A. Herrebout[a]*

[a] Department of Chemistry, University of Antwerp, Groenenborgerlaan 171, 2020 Antwerp (Belgium), E-mail: wouter.herrebout@uantwerpen.be

Electronic supplementary information

Table S1.1: Cartesian coordinates of the MP2/aug-cc-pVDZ optimized geometry of 2,2,4,4-Tetrafluoro-1,3-dithiethane ($C_2F_4S_2$).

D_{2h}	X	Y	Z
$C_2F_4S_2$			
S	0.000000	1.387164	0.000000
C	1.191095	0.000000	0.000000
F	2.014655	0.000000	1.085309
F	2.014655	0.000000	-1.085309
S	0.000000	-1.387164	0.000000
C	-1.191095	0.000000	0.000000
F	-2.014655	0.000000	1.085309
F	-2.014655	0.000000	-1.085309

Table S1.2: Cartesian coordinates of the MP2/aug-cc-pVDZ optimized geometry of TMP.

C_{3v}	X	Y	Z
TMP			
P	0.000000	0.000000	0.618978
C	0.000000	1.626598	-0.285498
H	-0.889964	2.208825	-0.001487
H	0.889964	2.208825	-0.001487
H	0.000000	1.481355	-1.378927
C	-1.408675	-0.813299	-0.285498
H	-1.467917	-1.875144	-0.001487
H	-2.357881	-0.333681	-0.001487
H	-1.282891	-0.740678	-1.378927
C	1.408675	-0.813299	-0.285498
H	2.357881	-0.333681	-0.001487
H	1.467917	-1.875144	-0.001487
H	1.282891	-0.740678	-1.378927

Table S1.3: Cartesian coordinates of the MP2/aug-cc-pVDZ optimized geometry of DMS.

C_{2v}	X	Y	Z
DMS			
S	0.000000	0.674247	0.000000
C	-1.370330	-0.522675	0.000000
H	-2.309643	0.047454	0.000000
H	-1.334542	-1.152689	-0.900834
H	-1.334542	-1.152688	0.900834
C	1.370330	-0.522675	0.000000
H	1.334542	-1.152689	-0.900834
H	2.309643	0.047454	0.000000
H	1.334542	-1.152689	0.900834

Table S2.1: Cartesian coordinates of the MP2/aug-cc-pVDZ optimized geometry of the chalcogen bonded complex between $C_2F_4S_2$ and dimethyl sulfide at the global minimum.

C_s	X	Y	Z
$C_2F_4S_2$			
S	0.191356	-0.733470	-0.170850
C	1.998971	-0.804876	0.120000
F	2.675866	-1.503257	-0.838102
F	2.334294	-1.398324	1.303986
S	2.355308	0.986928	0.089336
C	0.548378	1.061456	-0.190256
F	0.218467	1.672270	-1.359591
F	-0.104439	1.757456	0.786727
DMS			
S	-2.859015	0.181457	-0.363551
C	-3.235859	-1.581365	-0.605585
H	-4.248327	-1.810630	-0.243224
H	-3.182924	-1.788818	-1.683338
H	-2.498517	-2.208496	-0.080780
C	-2.998860	0.219438	1.450564
H	-2.265451	-0.463617	1.904766
H	-2.782994	1.245794	1.777093
H	-4.017638	-0.054091	1.761016

Table S2.2: Cartesian coordinates of the MP2/aug-cc-pVDZ optimized geometry of the chalcogen bonded complex between $C_2F_4S_2$ and dimethyl sulfide at the local minimum.

C_s	X	Y	Z
$C_2F_4S_2$			
S	0.483353	-0.877370	-0.433442
C	2.251251	-0.541287	-0.092591
F	3.053797	-0.702704	-1.184430
F	2.782383	-1.350728	0.870443
S	2.105149	1.202043	0.438060
C	0.337593	0.856257	0.124666
F	-0.209630	1.690191	-0.804410
F	-0.432023	1.008326	1.245986
DMS			
S	-2.792931	-0.675882	-0.586140
C	-3.024137	-1.291501	1.111104
H	-4.092611	-1.309448	1.370344
H	-2.628175	-2.315927	1.148773
H	-2.469421	-0.664377	1.823782
C	-3.475305	0.994150	-0.348929
H	-2.909878	1.532429	0.424861
H	-3.377866	1.529499	-1.303355
H	-4.538355	0.935700	-0.073858

Table S2.3: Cartesian coordinates of the MP2/aug-cc-pVDZ optimized geometry of the chalcogen bonded complex between $C_2F_4S_2$ and trimethylphosphine.

C_s	X	Y	Z
$C_2F_4S_2$			
S	-0.746085	-0.943557	-0.171824
C	-0.732578	0.878359	-0.018044
F	-0.185704	1.519432	-1.090931
F	-0.036342	1.334175	1.068263
S	-2.531490	1.164174	0.132565
C	-2.550666	-0.657026	-0.024279
F	-3.261768	-1.093164	-1.105756
F	-3.113856	-1.280533	1.052831
TMP			
P	2.558113	-0.347296	-0.089767
C	3.200323	1.336227	-0.535494
H	3.088853	1.499781	-1.618090
H	2.609212	2.103553	-0.013508
H	4.262389	1.446135	-0.259685
C	3.884403	-1.394855	-0.860612
H	3.746514	-2.445621	-0.563728
H	3.809639	-1.338031	-1.957123
H	4.889070	-1.062438	-0.550509
C	3.103800	-0.418643	1.683307
H	2.500793	0.283101	2.279263
H	2.939954	-1.431734	2.081225
H	4.170424	-0.158729	1.787862

Table S3: MP2/aug-cc-pVDZ ΔE(DZ) and CCSD(T)/CBS extrapolated complexation energies ΔE(CCSD(T)), calculated vapor phase complexation enthalpies Δ*H*° (vap,calc), the calculated complexation enthalpies in liquid krypton (Δ*H*° (LKr,calc)) and the corresponding experimentally obtained complexation enthalpy (Δ*H*° (LKr)) (kJ mol^{-1}) of the chalcogen bonded complexes between $C_2F_4S_2$ and dimethyl ether. All data are taken from Reference 36.

	S···O Chalcogen bonded complexes	
	Global Minimum	Local Minimum
Δ*E* (DZ)	-23.4	-22.2
Δ*E* (CCSD(T))	-25.0	-23.5
Δ*H*° (vap,calc)	-22.1	-20.8
Δ*H*° (LKr,calc)	-16.6	-15.2
Experimental		
Δ*H*° (LKr)	-13.5(1)	

Table S4: MP2/aug-cc-pVDZ vibrational frequencies, in cm^{-1}, infrared intensities, in km mol^{-1}, and Raman intensities, in $Å^4$ amu^{-1}, for the chalcogen bonded complex between $C_2F_4S_2$ and DMS and both monomers, as well as the complexation shift Δν.

	Monomer			Chalcogen bonded complex, global minimum			
	Frequency	IR int.	Raman int.	Frequency	Δν	IR int.	Raman int.
$C_2F_4S_2$							
ν_1 (A_g)	1160.9	0.0	8.6	1157.0	-4.0	5.4	7.7
ν_2 (A_g)	651.0	0.0	15.5	648.1	-2.8	1.0	20.3
ν_3 (A_g)	513.3	0.0	14.7	512.0	-1.4	1.4	33.7
ν_4 (A_g)	323.4	0.0	3.0	323.9	0.5	0.4	3.0
ν_5 (A_u)	231.2	0.0	0.0	235.0	3.8	0.03	0.004
ν_6 (B_{1g})	839.9	0.0	8.4	835.7	-4.3	6.4	22.4
ν_7 (B_{1g})	422.6	0.0	5.3	424.3	1.7	1.4	14.9
ν_8 (B_{1u})	1095.1	320.6	0.0	1088.9	-6.2	277.2	0.2
ν_9 (B_{1u})	428.3	0.4	0.0	430.0	1.7	0.3	0.0
ν_{10} (B_{1u})	56.3	1.2	0.0	60.0	3.7	1.0	0.1
ν_{11} (B_{2g})	1079.3	0.0	4.9	1073.8	-5.5	106.5	3.4
ν_{12} (B_{2g})	377.9	0.0	1.3	381.8	3.9	0.0	1.2
ν_{13} (B_{2u})	970.0	128.0	0.0	964.7	-5.3	139.1	5.8
ν_{14} (B_{2u})	335.3	4.5	0.0	335.8	0.6	8.9	1.8
ν_{15} (B_{3g})	282.2	0.0	2.1	286.6	4.4	0.0008	1.9
ν_{16} (B_{3u})	1065.2	732.2	0.0	1059.3	-5.9	562.2	3.9
ν_{17} (B_{3u})	638.7	15.9	0.0	636.3	-2.4	8.8	5.2
ν_{18} (B_{3u})	445.4	2.1	0.0	444.5	-0.9	5.7	3.6
DMS							
ν_1 (A_1)	3186.3	9.8	92.1	3188.4	2.0	4.6	73.2
ν_2 (A_1)	3062.2	31.8	338.0	3059.6	-2.6	26.2	273.4
ν_3 (A_1)	1473.5	0.3	7.6	1471.0	-2.5	2.9	9.1
ν_4 (A_1)	1352.5	0.8	0.9	1351.6	-0.9	0.1	7.6
ν_5 (A_1)	1046.4	8.6	0.4	1047.0	0.6	10.3	0.6
ν_6 (A_1)	713.3	2.8	22.1	711.6	-1.7	3.4	17.4
ν_7 (A_1)	260.8	0.03	3.0	262.6	1.8	0.07	2.5
ν_8 (A_2)	3168.0	0.0	16.5	3168.1	0.0	1.9	27.9
ν_9 (A_2)	1450.1	0.0	10.3	1447.6	-2.5	0.2	9.1
ν_{10} (A_2)	945.6	0.0	0.1	948.8	3.2	0.007	0.5
ν_{11} (A_2)	171.2	0.0	0.1	174.8	3.6	0.04	0.2
ν_{12} (B_1)	3159.9	21.3	119.4	3159.5	-0.4	18.9	107.3
ν_{13} (B_1)	1462.5	12.9	0.02	1460.2	-2.3	12.2	0.6
ν_{14} (B_1)	982.7	4.1	0.006	984.8	2.1	8.6	0.8
ν_{15} (B_1)	187.1	0.8	0.09	192.0	4.9	2.1	0.5
ν_{16} (B_2)	3187.4	3.4	42.0	3192.5	5.1	2.8	44.8
ν_{17} (B_2)	3066.9	26.3	2.8	3065.3	-1.6	18.9	45.3
ν_{18} (B_2)	1464.2	13.6	0.03	1461.2	-3.0	10.5	0.4
ν_{19} (B_2)	1326.0	6.5	0.1	1325.5	-0.4	3.4	0.2
ν_{20} (B_2)	912.7	0.2	0.2	915.1	2.4	0.2	0.2
ν_{21} (B_2)	765.1	0.1	8.5	763.1	-1.9	0.5	6.9

Van der Waals vibrations: 22.3 cm^{-1}, 0.8 km mol^{-1}, 0.5 $Å^4$ amu^{-1}, 40.4 cm^{-1}, 0.7 km mol^{-1}, 0.4 $Å^4$ amu^{-1}, 53.6 cm^{-1}, 0.1 km mol^{-1}, 0.3 $Å^4$ amu^{-1}, 71.7 cm^{-1}, 1.2 km mol^{-1}, 1.5 $Å^4$ amu^{-1}, 89.6 cm^{-1}, 0.03 km mol^{-1}, 1.4 $Å^4$ amu^{-1}, 122.3 cm^{-1}, 11.2 km mol^{-1}, 4.6 $Å^4$ amu^{-1}.

Table S5: MP2/aug-cc-pVDZ vibrational frequencies, in cm^{-1}, infrared intensities, in km mol^{-1}, and Raman intensities, in $Å^4$ amu^{-1}, for the chalcogen bonded complex between $C_2F_4S_2$ and DMS and both monomers, as well as the complexation shift Δν.

	Monomer			Chalcogen bonded complex, local minimum			
	Frequency	IR int.	Raman int.	Frequency	Δν	IR int.	Raman int.
$C_2F_4S_2$							
ν_1 (A_g)	1160.9	0.0	8.6	1155.4	-5.5	6.6	6.8
ν_2 (A_g)	651.0	0.0	15.5	647.7	-3.3	0.7	20.6
ν_3 (A_g)	513.3	0.0	14.7	512.5	-0.8	0.8	27.6
ν_4 (A_g)	323.4	0.0	3.0	324.5	1.1	0.4	3.5
ν_5 (A_u)	231.2	0.0	0.0	235.6	4.4	0.03	0.02
ν_6 (B_{1g})	839.9	0.0	8.4	837.8	-2.2	6.2	23.3
ν_7 (B_{1g})	422.6	0.0	5.3	423.9	1.3	0.8	13.5
ν_8 (B_{1u})	1095.1	320.6	0.0	1084.0	-11.1	274.8	0.4
ν_9 (B_{1u})	428.3	0.4	0.0	430.1	1.8	0.4	0.02
ν_{10} (B_{1u})	56.3	1.2	0.0	64.7	8.4	1.1	0.06
ν_{11} (B_{2g})	1079.3	0.0	4.9	1069.6	-9.7	161.7	3.3
ν_{12} (B_{2g})	377.9	0.0	1.3	381.8	3.9	0.07	1.1
ν_{13} (B_{2u})	970.0	128.0	0.0	966.7	-3.3	133.4	2.9
ν_{14} (B_{2u})	335.3	4.5	0.0	335.9	0.7	8.1	0.9
ν_{15} (B_{3g})	282.2	0.0	2.1	286.4	4.2	0.006	1.8
ν_{16} (B_{3u})	1065.2	732.2	0.0	1055.6	-9.7	542.8	3.3
ν_{17} (B_{3u})	638.7	15.9	0.0	636.4	-2.3	9.6	3.4
ν_{18} (B_{3u})	445.4	2.1	0.0	444.9	-0.5	6.0	2.4
DMS							
ν_1 (A_1)	3186.3	9.8	92.1	3188.3	2.0	5.3	57.8
ν_2 (A_1)	3062.2	31.8	338.0	3066.4	4.2	26.0	305.9
ν_3 (A_1)	1473.5	0.3	7.6	1472.5	-1.0	1.7	7.8
ν_4 (A_1)	1352.5	0.8	0.9	1351.7	-0.8	0.9	4.9
ν_5 (A_1)	1046.4	8.6	0.4	1046.9	0.6	15.6	0.9
ν_6 (A_1)	713.3	2.8	22.1	710.8	-2.5	3.8	19.0
ν_7 (A_1)	260.8	0.03	3.0	261.6	0.8	0.02	2.5
ν_8 (A_2)	3168.0	0.0	16.5	3176.4	8.4	0.3	18.7
ν_9 (A_2)	1450.1	0.0	10.3	1448.3	-1.8	0.4	9.5
ν_{10} (A_2)	945.6	0.0	0.1	948.7	3.1	0.07	0.4
ν_{11} (A_2)	171.2	0.0	0.1	172.9	1.7	0.1	0.2
ν_{12} (B_1)	3159.9	21.3	119.4	3169.4	9.5	14.5	121.5
ν_{13} (B_1)	1462.5	12.9	0.02	1461.0	-1.6	14.1	0.3
ν_{14} (B_1)	982.7	4.1	0.006	985.6	3.0	14.0	0.04
ν_{15} (B_1)	187.1	0.8	0.09	186.0	-1.1	1.5	0.4
ν_{16} (B_2)	3187.4	3.4	42.0	3192.0	4.6	3.2	49.3
ν_{17} (B_2)	3066.9	26.3	2.8	3071.1	4.2	20.4	28.3
ν_{18} (B_2)	1464.2	13.6	0.03	1462.5	-1.6	10.0	0.1
ν_{19} (B_2)	1326.0	6.5	0.1	1325.1	-0.9	4.1	0.2
ν_{20} (B_2)	912.7	0.2	0.2	915.3	2.5	0.2	0.3
ν_{21} (B_2)	765.1	0.1	8.5	763.4	-1.7	0.5	7.3

Van der Waals vibrations: 23.2 cm^{-1}, 0.5 km mol^{-1}, 0.2 $Å^4$ amu^{-1}, 44.7 cm^{-1}, 0.1 km mol^{-1}, 0.8 $Å^4$ amu^{-1}, 61.9 cm^{-1}, 1.1 km mol^{-1}, 0.9 $Å^4$ amu^{-1}, 71.2 cm^{-1}, 0.5 km mol^{-1}, 1.0 $Å^4$ amu^{-1}, 83.0 cm^{-1}, 0.6 km mol^{-1}, 1.5 $Å^4$ amu^{-1}, 103.9 cm^{-1}, 7.9 km mol^{-1}, 1.5 $Å^4$ amu^{-1}.

Table S6: MP2/aug-cc-pVDZ vibrational frequencies, in cm^{-1}, infrared intensities, in km mol^{-1}, and Raman intensities, in $Å^4$ amu^{-1}, for the chalcogen bonded complex between $C_2F_4S_2$ and TMP and both monomers, as well as the complexation shift Δν.

	Monomer			Chalcogen bonded complex			
	Frequency	IR int.	Raman int.	Frequency	Δν	IR int.	Raman int.
$C_2F_4S_2$							
ν_1 (A_g)	1160.9	0.0	8.6	1153.5	-7.4	6.9	7.1
ν_2 (A_g)	651.0	0.0	15.5	646.6	-4.3	1.5	23.7
ν_3 (A_g)	513.3	0.0	14.7	511.2	-2.1	1.2	37.4
ν_4 (A_g)	323.4	0.0	3.0	323.9	0.5	0.8	4.5
ν_5 (A_u)	231.2	0.0	0.0	235.5	4.3	0.04	0.04
ν_6 (B_{1g})	839.9	0.0	8.4	836.8	-3.1	10.2	31.7
ν_7 (B_{1g})	422.6	0.0	5.3	423.5	0.9	1.2	19.2
ν_8 (B_{1u})	1095.1	320.6	0.0	1081.6	-13.6	275.2	0.4
ν_9 (B_{1u})	428.3	0.4	0.0	429.8	1.5	0.3	0.0
ν_{10} (B_{1u})	56.3	1.2	0.0	60.8	4.5	0.9	0.1
ν_{11} (B_{2g})	1079.3	0.0	4.9	1065.7	-13.6	120.1	4.6
ν_{12} (B_{2g})	377.9	0.0	1.3	381.8	3.9	0.1	0.9
ν_{13} (B_{2u})	970.0	128.0	0.0	966.8	-3.2	84.8	20.3
ν_{14} (B_{2u})	335.3	4.5	0.0	334.9	-0.4	9.6	2.2
ν_{15} (B_{3g})	282.2	0.0	2.1	286.6	4.4	0.009	1.8
ν_{16} (B_{3u})	1065.2	732.2	0.0	1054.9	-10.4	594.9	8.1
ν_{17} (B_{3u})	638.7	15.9	0.0	635.2	-3.5	8.1	7.5
ν_{18} (B_{3u})	445.4	2.1	0.0	444.0	-1.4	7.3	4.8
TMP							
ν_1 (A_1)	3148.5	33.6	160.8	3152.0	3.5	26.9	175.0
ν_2 (A_1)	3043.5	29.4	528.4	3046.7	3.1	38.5	556.7
ν_3 (A_1)	1469.0	9.2	1.5	1467.7	-1.3	7.5	1.4
ν_4 (A_1)	1314.7	5.1	7.3	1315.0	0.3	3.2	14.3
ν_5 (A_1)	957.8	20.1	5.0	957.2	-0.7	106.2	13.9
ν_6 (A_1)	660.9	0.5	26.5	662.8	1.9	0.7	25.5
ν_7 (A_1)	287.5	1.0	1.5	287.2	-0.4	1.3	1.2
ν_8 (A_2)	3168.1	0.0	0.0	3171.1	3.0	2.9	30.0
ν_9 (A_2)	1440.1	0.0	0.0	1439.0	-1.1	0.02	0.2
ν_{10} (A_2)	776.6	0.0	0.0	779.8	3.2	0.002	0.006
ν_{11} (A_2)	164.1	0.0	0.0	164.7	0.6	0.002	0.008
ν_{12} (E)	3167.9	11.5	95.9	3172.3	4.4	6.5	63.1
ν_{13} (E)	3149.3	3.0	18.4	3153.5	4.2	4.4	35.6
ν_{14} (E)	3046.9	16.7	4.2	3050.0	3.1	12.9	16.8
ν_{15} (E)	1456.7	8.7	3.0	1455.6	-1.1	8.5	3.6
ν_{16} (E)	1446.2	3.1	9.5	1445.0	-1.2	2.2	8.4
ν_{17} (E)	1290.0	2.3	0.7	1290.4	0.5	3.1	0.6
ν_{18} (E)	946.6	16.5	0.5	949.0	2.5	14.0	0.5
ν_{19} (E)	831.0	0.2	0.3	832.7	1.8	0.6	1.9
ν_{20} (E)	718.3	11.6	11.8	725.3	7.0	9.2	12.6
ν_{21} (E)	249.8	0.2	2.8	246.3	-3.5	0.3	2.5
ν_{22} (E)	207.4	0.0009	0.6	207.3	0.0	0.004	0.4

Van der Waals vibrations: 16.5 cm^{-1}, 0.05 km mol^{-1}, 0.2 $Å^4$ amu^{-1}, 24.6 cm^{-1}, 0.3 km mol^{-1}, 0.4 $Å^4$ amu^{-1}, 39.3 cm^{-1}, 1.4 km mol^{-1}, 0.6 $Å^4$ amu^{-1}, 59.4 cm^{-1}, 0.6 km mol^{-1}, 2.0 $Å^4$ amu^{-1}, 72.7 cm^{-1}, 0.2 km mol^{-1}, 0.5 $Å^4$ amu^{-1}, 80.0 cm^{-1}, 0.1 km mol^{-1}, 1.9 $Å^4$ amu^{-1}.

Table S7: Overview of the different van 't Hoff plots constructed for the chalcogen bonded complex between $C_2F_4S_2$ and DME in LKr in the 121-155 K temperature interval, showing the estimated mole fractions of each monomer, range of the integrated monomer and complex bands and complex enthalpies $\Delta H°$ (LKr).

$x_{C_2F_4S_2}$	x_{DMS}	Integrated $C_2F_4S_2$ band (cm^{-1})	Integrated DMS band (cm^{-1})	Integrated Complex band (cm^{-1})	$\Delta H°$ (LKr) [a]
9.4×10^{-5}	1.9×10^{-3}	1125-1058	1345-1290	1073.2-1055	-12.97(8)
9.4×10^{-5}	1.9×10^{-3}	970.5-950.3	1080-945	965-950	-12.4(1)
3.8×10^{-5}	1.4×10^{-3}	1125-1096.7	998-952	1073-1055	-12.0(1)
3.8×10^{-5}	1.4×10^{-3}	973-950.5	1053-1006	962-953.5	-12.5(1)
1.9×10^{-3}	1.1×10^{-3}	968.5-952	1065-1002	963.5-952	-12.5(3)
1.9×10^{-4}	5.6×10^{-4}	1127-1096.8	1480-1395	966-951	-11.7(2)
1.9×10^{-4}	5.6×10^{-4}	974-950.2	3025-2815	1111-1094.5	-12.00(4)

[a] Values are given with the standard deviation of the linear regression in parentheses.

Table S8: Overview of the different van 't Hoff plots constructed for the chalcogen bonded complex between $C_2F_4S_2$ and TMP in LKr in the 121-155 K temperature interval, showing the estimated mole fractions of each monomer, range of the integrated monomer and complex bands and complex enthalpies $\Delta H°$ (LKr).

$x_{C_2F_4S_2}$	x_{DMS}	Integrated $C_2F_4S_2$ band (cm^{-1})	Integrated TMP band (cm^{-1})	Integrated Complex band (cm^{-1})	$\Delta H°$ (LKr) [a]
1.9×10^{-4}	1.9×10^{-3}	1122-1096.5	3010-2930.5	964-943.4	-13.1(1)
2.8×10^{-5}	1.1×10^{-3}	970-952	3010-2930.5	1120-1040	-12.85(5)
9.4×10^{-5}	1.0×10^{-3}	1127-1096.8	3010-2930.5	1112-1076.8	-12.73(4)
9.4×10^{-5}	1.0×10^{-3}	970-952	1460-1400	963-943	-12.96(6)
1.9×10^{-5}	1.1×10^{-3}	1127-1096.8	1330-1260	1112.5-1051.7	-12.54(8)
3.8×10^{-4}	5.6×10^{-4}	659.7-644.1	1460-1400	1441-1413	-13.82(5)

[a] Values are given with the standard deviation of the linear regression in parentheses.

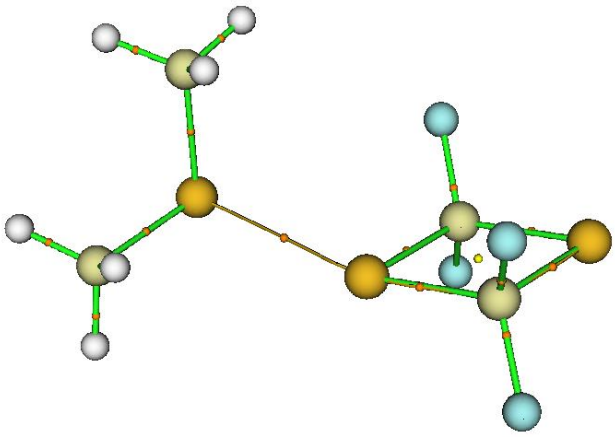

electron densities, in a.u., at the bond critical point : S···S 0.0155

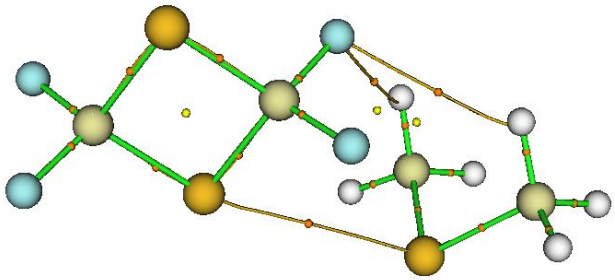

electron densities, in a.u., at the bond critical points : S···S 0.0129
F…H 0.0046
F…H 0.0051

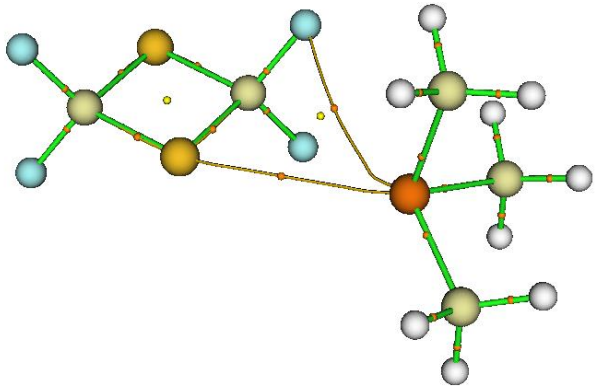

electron densities, in a.u., at the bond critical points : S···P 0.0131
F···P 0.0068

Figure S1. Bond critical points (orange), ring critical points (yellow) and bond paths for the complexes of $C_2F_4S_2$ with dimethyl sulfide and trimethylphosphine. All results are obtained using the MP2/aug-cc-pVDZ electron density.

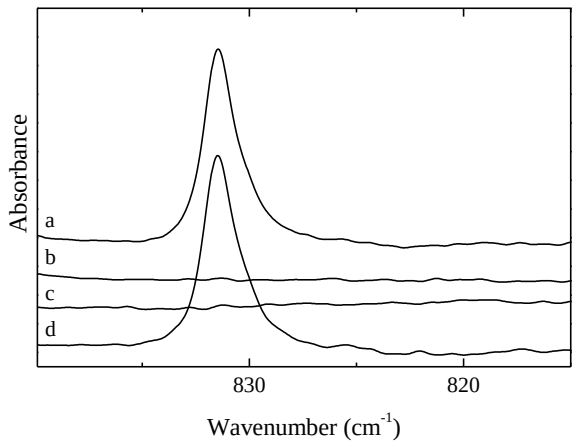

Figure S2: Infrared spectra of the $C_2F_4S_2$ ν_6 spectral region for the mixtures of $C_2F_4S_2$ with TMP-d_9 dissolved in LKr at 133 K. In each panel, trace *a* represents the mixed solution, while traces *b* and *c* show the rescaled spectra of the solutions containing only $C_2F_4S_2$ or TMP-d_9, respectively. Trace *d* represents the spectrum of the complex which is obtained by subtracting the rescaled traces *b* and *c* from trace *a*. Estimated mole fractions of the solutions of the mixture are 3.8×10^{-4} for $C_2F_4S_2$ and 9.4×10^{-4} for TMP-d_9.